Miniaturizing Ultrastable Electromagnetic Oscillators: Sub-10^{-14} Frequency Instability from a Centimeter-Scale Fabry-Perot Cavity

Charles A. McLemore[1,2,*] Naijun Jin,[3] Megan L. Kelleher,[1,2] James P. Hendrie,[1,2]
David Mason,[3] Yizhi Luo,[3] Dahyeon Lee,[1,2] Peter Rakich,[3] Scott A. Diddams,[1,2,4] and
Franklyn Quinlan[1,2,†]

[1]*Department of Physics, University of Colorado Boulder, Boulder, Colorado 80309, USA*
[2]*National Institute of Standards and Technology, Boulder, Colorado 80305, USA*
[3]*Department of Applied Physics, Yale University, New Haven, Connecticut 06520, USA*
[4]*Department of Electrical, Computer and Energy Engineering, University of Colorado Boulder, Boulder, Colorado 80309, USA*

The best performance from compact, portable, and repeatably manufactured electromagnetic (EM) oscillators has for decades been built upon crystalline quartz resonators operating at radio frequencies. Such a source of frequency-stable EM waves has enabled a wide range of applications of significant technical and societal benefit, such as navigation and communication systems, distributed sensing, geodesy, and fundamental physics. However, meeting demands for increased measurement sensitivity requires pushing beyond a fractional frequency stability of 10^{-13}, typical of the best ovenized quartz. To date, such performance has been available in the microwave domain only with the use of complex cryogenic systems, or in the optical domain at the expense of larger volume and weight. In either case, the size, weight, and power of state-of-the-art EM oscillators has relegated their use to laboratory experiments. Here we demonstrate the validity of a manufacturable, compact Fabry-Perot reference that improves upon all other centimeter-scale oscillators by more than a factor of 10, including those based on solid-state optical resonators as well as quartz. In a specific implementation, we show an 8 ml bonded assembly containing three vacuum-gap Fabry-Perot optical cavities with mirrors lithographically fabricated on a single substrate, each with quality factor exceeding 10 billion. A laser stabilized to one of the cavities exhibits thermal-noise-limited phase noise for offset frequencies ranging from 1 Hz to nearly 1 kHz, and fractional frequency stability of 7×10^{-15} at 1 s. Our advance with lithographically defined and microfabricated mirrors is validated by rigorous models, which highlight a path to oscillators with size comparable to ovenized quartz, but with significantly improved performance. For example, we predict sub-10^{-14} performance is readily attainable with a Fabry-Perot cavity volume less than 2 ml.

I. INTRODUCTION

Highly frequency-stable electromagnetic (EM) waves are foundational for a vast number of applications across science and technology, including optical atomic clocks [1–4], gravitational wave detection [5], low-noise microwave generation [6,7], and distributed sensing [8,9], with applications in fundamental physics [10–13], coherent radar [14,15], and the redefinition of the SI second [16]. While some of these applications are amenable to laboratory-based studies, a growing number require compact, portable, and repeatably manufactured sources of ultrastable EM waves in the field, such as ground-based geodesy [17,18], earthquake detection [19], and space-based tests of fundamental physics [20].

The highest frequency stability microwave oscillators derive their stability from cryogenic whispering gallery mode resonators, whereas the highest stability optical resonators, both at room and cryogenic temperatures, rely on vacuum-gap Fabry-Perot cavities. State-of-the-art optical systems have demonstrated laser linewidths below 10 mHz and fractional frequency instability as low as 4×10^{-17} [21], corresponding to absolute length fluctuations on the scale of a proton diameter. Furthermore, optical frequency combs can be leveraged to transfer this fractional frequency stability to other frequency bands across the EM spectrum. However, this level of performance is achieved by exploiting large cavity mode volumes and/or cryogenic temperatures, relegating these systems to well-controlled

*charles.mclemore@colorado.edu
†franklyn.quinlan@nist.gov

laboratory environments. Cryogenic microwave systems, which have demonstrated fractional frequency stability as low as 2×10^{-16} [22], likewise have infrastructure requirements that diminish out-of-the-lab utility.

In compact and portable systems, radio-frequency (rf) quartz oscillators have remained the "gold standard" for decades, finding ubiquitous application in areas such as communications, radar, navigation, and timekeeping. Temperature-stabilized (or "ovenized"), quartz oscillators have demonstrated fractional frequency instability near 10^{-13} at 1 s [23]. This frequency stability can also be translated to the optical domain with the use of an optical frequency comb, as recently demonstrated in a compact platform with high optical frequency tunability [24]. The pursuit of a compact oscillator with frequency stability better than 10^{-13} has led to a proliferation of different optical dielectric resonator designs [25–29]. However, the fundamental limit imposed by thermorefractive noise [30] has to date prevented these resonators from substantially outperforming existing ovenized quartz technology [Fig. 1(a)]. Furthermore, their high susceptibility to long-term thermal drift often necessitates temperature control at the nanokelvin level to maintain frequency stability near the thermorefractive limit. The temperature stabilization and vacuum employed in many of the best performing systems allow for a large degree of environmental isolation,

but also increase overall system volumes. To facilitate fair comparison of these different frequency references, the legend of Fig. 1(a) notes the extent of environmental isolation employed in each system.

Vacuum-gap Fabry-Perot cavities avoid much of the thermorefractive noise that limits the performance of solid-state dielectric resonators. Furthermore, Fabry-Perot cavities can be constructed with low thermal expansion materials that greatly reduce their temperature sensitivity, enabling low thermal drift on long timescales. The frequency stability of lasers locked to select state-of-the-art compact Fabry-Perot cavities [31,32] is also shown in Fig. 1(a), where it can be seen that the instability is at least an order of magnitude lower than that of solid-state dielectric resonators. This improved performance comes at the expense of a larger cavity volume, small-batch lap and polish manufacturing, and individual hand assembly. Thus, the ideal portable oscillator would inherit the frequency stability of bulk Fabry-Perot reference cavities but with compactness and manufacturability associated with dielectric resonator designs.

In this paper, we present a near 1 million finesse Fabry-Perot reference cavity constructed with lithographically fabricated micromirrors. The fabrication process allows for highly parallel manufacture of mirrors on a single substrate with user-defined radius of curvature. An 8-ml optical
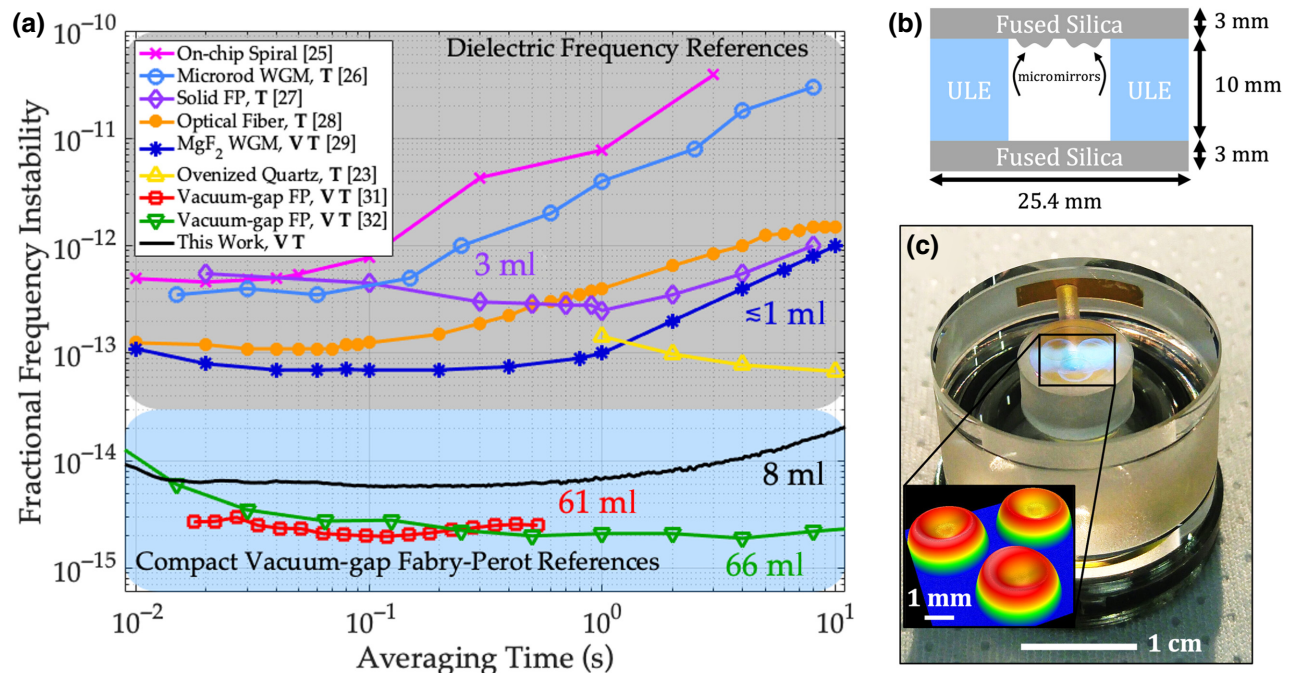

FIG. 1.   (a) Comparison of existing compact frequency reference technologies. FP, Fabry-Perot cavity; WGM, whispering-gallery-mode resonator. Bold text in the legend indicates which results relied on vacuum (**V**) and/or active temperature control (**T**). (b) Cross section of the finalized cavity assembly with an overall volume of 8 ml. ULE, ultralow expansion glass. (c) Photograph of the reference cavity. Inset: surface profile data of the three micromirrors fabricated on a single substrate. Color scale on the inset ranges from 0 μm (blue) to 0.75 μm (red).

contact bonded assembly, consisting of three high-finesse optical cavities, is shown schematically in Fig. 1(b) and pictured in Fig. 1(c). We confirm the cavity thermal noise is not adversely affected by the manufacturing process, with the phase noise of a laser locked to the cavity operating at the predicted thermal-noise limit out to kHz offset frequencies. The corresponding fractional frequency instability is close to the thermal limit of 5×10^{-15} and is better than 10^{-14} up to several seconds of averaging, representing an order of magnitude improvement over existing oscillators based upon centimeter-scale resonators. Furthermore, we use finite-element simulation to explore the cavity design space opened up by lithographic mirror fabrication, predicting thermal noise and cavity thermal expansion as a function of mirror substrate thickness. Based on these thermal-noise simulations, we identify a path to reduce the cavity volume to only 2 ml without sacrificing the level of noise performance achieved in the current 8-ml assembly. Through this demonstration of a microfabricated mirror-based optical reference cavity, we aim to show that a generation of mass-produced, miniature Fabry-Perot cavities presents the most compelling path towards widely available ultrastable frequency references for field-based experiments.

II. NOISE MODELING AND CAVITY DESIGN

A. Mirror design and fabrication

Several compact Fabry-Perot cavity designs have been proposed and demonstrated to specifically address the need for portability while meeting high stability requirements [31–34]. These cavities exploit a high degree of mechanical symmetry to reduce acceleration and holding force sensitivity and use large radius-of-curvature (ROC) mirrors to reduce the cavity thermal-noise limit. However, these cavities are individually hand assembled and use standard lap and polish techniques to fabricate a curved surface on the glass mirror substrates—a process with no clear path towards mass manufacturability. To permit bonding of a traditionally polished substrate to a planar cavity spacer, it is further necessary to polish a flat annulus on the outer rim of the mirror. Both the curved mirror surface and bonding annulus are readily created using our lithographic techniques, as we describe here.

Our mirror fabrication process utilizes photoresist reflow and etching to form mm-scale diameter micromirrors with customizable ROC [35,36]. The process consists of patterning a disk of photoresist onto a superpolished glass substrate, which is then exposed to a solvent vapor reflow in a custom chamber. Gradually, the solvent vapor is absorbed into the photoresist, which begins to flow as surface tension reshapes the disk, causing an approximately parabolic dimple to form in the center. Fine tuning of the reflow duration along with the initial dimensions of the photoresist disk allow for a wide range of mirror curvatures

to be achieved with this technique; parabolic surfaces have been produced with radii of curvature ranging from less than 1 mm to over 1 m. Following the reflow step, a reactive ion etch is used to transfer the parabolic micromirror shape from the photoresist into the glass substrate below with angstrom-level surface roughness. Finally, a highly reflective dielectric mirror coating is applied via ion-beam sputtering to complete the micromirror. Full details of this process are available in Ref. [36]. Since the photoresist is applied lithographically and the whole substrate is etched at once, this technique allows for a high degree of parallel fabrication. Furthermore, the bonding annulus can be lithographically defined as well, leading to a high degree of repeatability in the cavity assembly.

Since we seek to demonstrate the viability of these microfabricated mirrors for use in ultrastable frequency references, we increase the ROC to approximately 1 m to maximize the intracavity optical spot size. This averages thermal fluctuations over a greater area on the mirror surfaces, thereby lowering the thermal noise floor [37]. Furthermore, to evaluate the repeatability and parallel manufacture capabilities of the micromirror fabrication technique, we include three individual large ROC micromirrors on a single mirror substrate, each capable of forming an optical cavity when paired with a single optical flat. To optimize the remainder of the cavity design, we perform finite-element simulations to assess both the thermal noise and temperature sensitivity of various geometries. With our microfabricated mirrors, the design space includes mirror-substrate thicknesses much less than that available with standard polished mirrors, as well as substrates with smaller cross-section diameter.

B. Noise modeling

The most crucial considerations in the cavity design are those that affect the thermal-noise floor, which must be below $1.3/f^3$ dBc/Hz (where f is the offset frequency) to reach fractional frequency instability of below 10^{-14}. Thermal noise in Fabry-Perot reference cavities is rooted in thermally driven stochastic fluctuations in the cavity mirrors and spacer. By individually considering how thermal fluctuations affect the length of the optical axis through different mechanisms, we can calculate the thermal-noise floor as the sum of these contributions. In our analysis, we consider Brownian noise arising from mechanical damping within the materials [37,38], thermoelastic noise resulting from the coupling of thermal fluctuations to a finite coefficient of thermal expansion (CTE) in the cavity materials [39,40], and thermorefractive noise due to a temperature-dependent index of refraction within the mirror coatings [41].

While analytical models exist to calculate these noise sources, the models often depend on simplifying assumptions that typically hold for bulk Fabry-Perot cavities. However, as we design more compact cavities, some of

these assumptions break down, particularly assuming the mirror substrates are large compared to the characteristic length scale of thermal diffusion. Following Ref. [38], we use finite-element analysis software (COMSOL) to construct a model of our cavity and apply a force to the mirrors with a Gaussian profile matching that of our optical mode. After computing the resulting deformation of the model cavity, we leverage the fluctuation-dissipation theorem [42] to extract the power spectral density of mirror surface fluctuations. Summing the contributions from Brownian, thermoelastic, and thermorefractive noise sources, we arrive at the total expected thermal noise of a given cavity design. As pointed out in Ref. [38], the Brownian noise from a small cavity spacer can be grossly underestimated when using simplified analytical models. We additionally find that, for the thin mirror substrates available with microfabrication, the Brownian noise of the coating and mirror substrate are affected by the contact area between the mirror substrate and spacer. A larger contact area tends to restrict the drumheadlike motion, driven by Brownian noise, that otherwise increases the mirror surface displacement. It is worth noting that in future designs, the inclusion of only a single micromirror will allow for a large reduction in cavity and bore-hole diameter, and therefore total volume, without sacrificing noise performance. By appropriately scaling down the inner and outer diameters of the spacer to maintain a comparable bonding area as a fraction of the total cross-section area, we can reduce the volume without increasing this drumheadlike substrate motion. Then, with the same spacer length as in the present design, we expect the cavity to experience comparable fractional length changes from the substrate motion, despite the reduced cavity volume. For example, reducing the cavity diameter by half to 12.7 mm would result in a cavity volume of only 2 ml while maintaining a comparable level of thermal noise.

C. Cavity thermal expansion

In addition to calculating the thermal-noise floor of the cavity, we also utilize finite-element simulations to determine the temperature sensitivity of various cavity designs. While stochastic thermal noise dominates the stability of a Fabry-Perot reference cavity at short timescales, temperature drift of the optical cavity length typically dominates over long timescales. To maintain sufficient fractional frequency stability over several seconds, it was therefore necessary to reduce the magnitude of the effective cavity CTE through careful design of the cavity geometry and materials. We focus our CTE simulations on a cavity structure that includes our test substrate with three micromirrors. This requires a total cavity diameter of 25.4 mm, with a 10-mm-diameter bore hole in the center, while the mirror-substrate thickness and material are left as free parameters. We then simulate the change in length of the

optical axis (sampled with a Gaussian profile matching the optical mode) as the temperature of the cavity is swept. The slope of this length change with respect to temperature is proportional to the cavity's effective CTE [43], which we use to evaluate the relative temperature sensitivity.

Using noise and temperature sensitivity simulations in conjunction, we consider several design trade-offs to arrive at a compact, low-noise design. For example, while using fused silica as the mirror-substrate material provides a lower thermal noise floor (due to the material's high mechanical quality factor Q_M and correspondingly low internal damping), fused silica's relatively large CTE also increases the magnitude of the effective cavity CTE when compared to other possible substrate materials like ultralow expansion (ULE) glass. This is predominantly a result of differentially greater radial expansion in the mirror substrates than the spacer causing bowing in the mirrors. To counteract this increased cavity CTE, we explore thinner mirror substrates, which improve the CTE, although making the substrates too thin results in a significant increase to the thermal noise (Fig. 2). Through these simulations, we also determine that a spacer length of 10 mm offers a good compromise, allowing a thermal noise limit below our goal of 10^{-14} fractional frequency instability, while keeping the overall cavity volume below 10 ml. Furthermore, we find that, for a given cavity outer diameter, increasing the bond area reduces the effective cavity CTE.

The ability to lithographically tailor the shape of the substrate surface allows us to overcome some of the limitations of conventional fabrication techniques. Considering the relevance of the optical contact bond area to both the noise and cavity CTE, it is worth noting the level of control our microfabrication technique provides over this
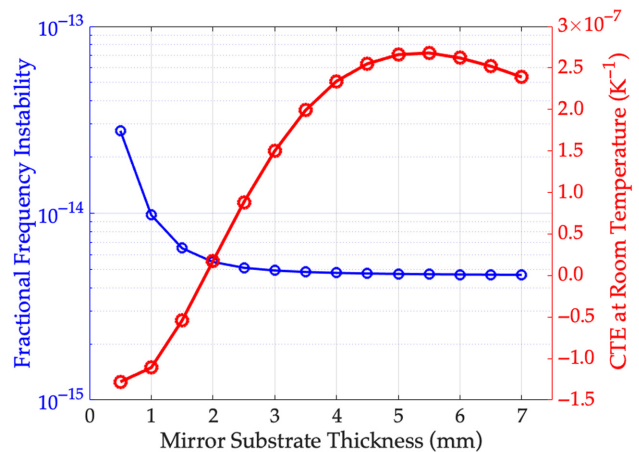
FIG. 2. Simulated trade-off between fractional frequency instability and cavity temperature sensitivity for various potential mirror-substrate thicknesses. The CTE zero crossing of the 10-mm ULE spacer used in the simulation is 45 °C, whereas the zero crossing of the ULE used in the experiment is specified at 45 °C ± 5 °C.

parameter. Two factors set the upper bound on the bond area: the spacer bore-hole diameter and the inner diameter of the mirror-substrate annulus. In our experience, standard curved mirrors created through lapping and polishing display significant variability in the mirror contact annulus, leading to unpredictability in CTE and thermal noise when forming bonded cavities. Additionally, large ROC mirrors have a central recess of only a few micrometers, with smaller mirror diameters yielding smaller recess for a given ROC. This puts a lower limit on the diameter of the mirror, since otherwise the annulus polishing will damage the pristine surface at the mirror's center. In our microfabrication procedure, an annular area around the edge of the substrate is protected with a thick coating of photoresist, blocking the reactive ion etch. This leaves an intact bonding annulus of precisely controlled area. Furthermore, this annulus protection scheme guarantees that the surface quality of the bonding area remains sufficient for optical contact bonding. As we push towards building more compact cavities with thinner mirror substrates, larger ROC, and smaller overall diameter, the precise control over bond area that this technique provides will be essential for repeatably achieving target performance. Combined with the numerical simulation methods discussed above, these tools will help realize an unexplored regime of compact cavities that push beyond traditional geometries where analytical solutions apply.

Implementing this annulus protection scheme, we finalize the cavity design with a 10-mm-long ULE spacer (CTE zero crossing: $45\,°C \pm 5\,°C$) to minimize thermal sensitivity with fused silica mirror substrates to provide sub-10^{-14} fractional frequency instability. The minimum substrate thickness we could readily obtain with suitably low roughness (for high finesse) and high surface figure (for optical contact bonding) is 3 mm. This choice of substrate thickness also provides a good compromise between noise and CTE. The completed cavity design is assembled by optical contact bonding the fused silica mirror substrates (with dielectric coating reflectivity $>99.999\%$) to the ULE spacer, resulting in an overall volume of 8 ml, effective CTE of 1.5×10^{-7} K^{-1} at room temperature, thermal phase noise floor of $-4.4/f^3$ dBc/Hz, and fractional frequency instability floor of 5×10^{-15}.

III. EXPERIMENTAL RESULTS AND DISCUSSION

A. Cavity finesse

For a compact cavity of short length, high finesse is particularly important to achieve a narrow cavity resonance, which enables greater rejection of electronic noise sources in the laser frequency lock [44] and improves rejection of frequency instabilities due to residual amplitude modulation [45]. The finesse is dependent on the mirror transmission and excess loss due to scattering, absorption, and beam clipping [46]. To maintain high finesse, it is

critical that the micromirror etching process does not degrade the original angstrom-level roughness of the superpolished substrate, as this could lead to excess scattering losses. Furthermore, while scattering and absorption are largely intrinsic to a given mirror, determined by the roughness of the surface and quality of the dielectric coating, significant additional beam-clipping loss can be introduced when rigidly bonding a cavity. Due to the mm-scale diameter of these micromirrors, even minor errors in parallelism (greater than approximately 400 microradians) between the end faces of the spacer can result in significant finesse reduction due to beam clipping. Small temperature gradients in the reflow chamber while forming the micromirror shapes could also introduce asymmetries and mirror tilt, which, once bonded to a rigid spacer, would transversely shift the position of the cavity's optical mode, incurring clipping losses as the optical mode overlaps the edge of the micromirror. Thus, while clipping losses are ultimately dependent on the spacer parallelism as well as the micromirror tilt, spacers machined with < 50 microradian parallelism are commercially available, which we calculate will contribute negligible ($< 10^{-15}$) excess optical loss per round trip. With other losses expected to be on the order of 10^{-6}, we are therefore concerned only with additional tilt that the micromirror fabrication process might add.

In light of these considerations, we ensure that the bonded cavity maintained consistently high finesse by performing cavity ringdown (CRD) measurements on all three micromirror cavities [47]. By measuring all three, we confirm that the micromirrors exhibit pristine surface quality and minimal tilt asymmetries with a high degree of repeatability. To perform the CRD measurements, we swept the frequency of a 1550-nm commercial fiber laser through a TEM_{00} mode of the cavity while sending the light through an acousto-optic modulator (AOM). When a photodetector monitoring the transmission through the cavity witnessed a spike in intensity, it triggered a high-speed switch, which cut off the rf power to the AOM, blocking the light incident on the cavity. We then monitor the exponential decay of resonant light out of the cavity using the transmission detector. With the exponential decay time constant τ (equivalent to the photon lifetime) and the cavity length L, we then determine the finesse as $F = \pi \tau c / L$, with c the speed of light in vacuum. Figure 3(a) shows CRD data for all three micromirror cavities, along with exponential fits, which are used to extract the photon lifetime in each case. To assess the repeatability of the measurement, we perform 20 CRD measurements on each micromirror. The results are presented in Fig. 3(b), with the average finesse of micromirrors 1, 2, and 3 being 980 000, 900 000, and 920 000, respectively. These correspond to linewidths of 15.3, 16.7, and 16.3 kHz. We separately measured the coating transmission to be approximately equal to 1.9 ppm [36], indicating single
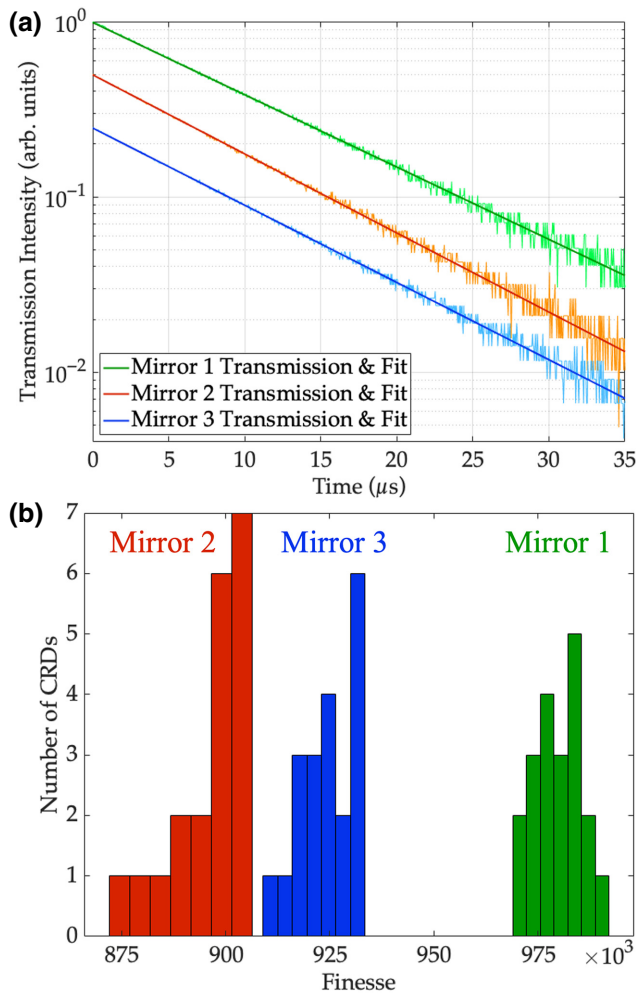
FIG. 3. (a) Cavity ringdown measurements for each of the three micromirror cavities (offset for clarity), including exponential fits used to extract the photon lifetime τ. (b) Histogram showing the repeatability of the cavity ringdown measurement for each micromirror, with mean values of 900 000, 920 000, and 980 000. Corresponding quality factors are 11.6, 11.9, and 12.6 billion.

mirror loss of the contacted cavity of only approximately 1.3, 1.6, and 1.5 ppm for mirrors 1, 2, and 3, respectively. In addition to the mirrors used to form this cavity assembly, over a dozen other mirrors are tested without bonding to spacers (allowing for optimal alignment), yielding a mean finesse value near 1 million and below 1-ppm scattering loss, with the highest finesse mirrors reaching 1.3 million [36]. These results confirm that the etching process does not introduce substantial scattering loss and rigid bonding of the fabricated substrates in a cavity introduces significantly less than 1 ppm of additional clipping loss per mirror. With finesse values consistently near 1 million, all three micromirrors are suitable for locking a laser at the thermal-noise limit.

B. Phase noise and frequency stability

Having established the high finesse of all three micromirrors, we choose the cavity formed by micromirror 3 for the remaining measurements since it has the largest ROC at 1.1 m, leading to the lowest thermal noise limit, as discussed in Sec. II. However, this thermal-noise limit in part depends on the high mechanical Q_M of the underlying fused silica used as a mirror substrate. While high Q phonon resonances in quartz have been demonstrated with a similar surface etch process [35], and the finesse measurements confirmed that the micromirror fabrication technique maintains the original surface quality of the substrate, it was also necessary to measure the fundamental thermal noise of the mirrors to confirm that the etch process used in the micromirror fabrication did not significantly degrade the Q_M of the substrates. For our cavity, the phase noise sensitivity to changes in Q_M is limited by the coating noise, estimated to be about 10 dB above the mirror-substrate noise. Thus, a tenfold reduction in Q_M would increase the total noise approximately 3 dB. Coatings with lower thermal noise [48] or a cavity with a larger spot size would reduce the separation between coating and substrate noise and increase the sensitivity to small changes in Q_M of the substrate.

Using the TEM$_{00}$ mode of the cavity formed by this mirror, we lock the output frequency of a 1550-nm fiber laser to the cavity using the Pound-Drever-Hall (PDH) method [49], depicted in Fig. 4(a). The output from a commercial fiber laser is sent through an AOM and an electro-optic modulator (EOM), which applies sidebands at 8 MHz. The light is then coupled to the cavity. The cavity assembly is housed in a rigid holding structure with a heat shield, and is held in a vacuum enclosure at 10^{-5} Pa with active temperature stabilization at 27 °C applied to the outside of the vacuum enclosure. For further environmental isolation, the entire apparatus is contained in an acoustic damping box with active vibration cancellation. The reflected signal from the cavity is photodetected and demodulated with a mixer to extract an error signal, which is filtered and amplified to feed back to both the laser and the AOM. Fast feedback is applied to the AOM via frequency modulation implemented with a voltage-controlled oscillator (VCO), while low-pass filtered slow feedback is applied to a piezoelectric tuning port on the laser. To measure the stability of the locked laser, stabilized light is split off after the AOM and divided into two channels for comparison with two optical frequency combs stabilized to independent ultrastable optical references [50]. Heterodyne beat notes from each arm are digitally sampled with software-defined radio (SDR) at 2 MSa/s and cross correlated to remove noise not common to both channels, leaving just the noise of the stabilized light [31,51]. As Fig. 4(b) shows, the phase noise of the stabilized light follows the simulated thermal-noise limit of the cavity out to around 1-kHz
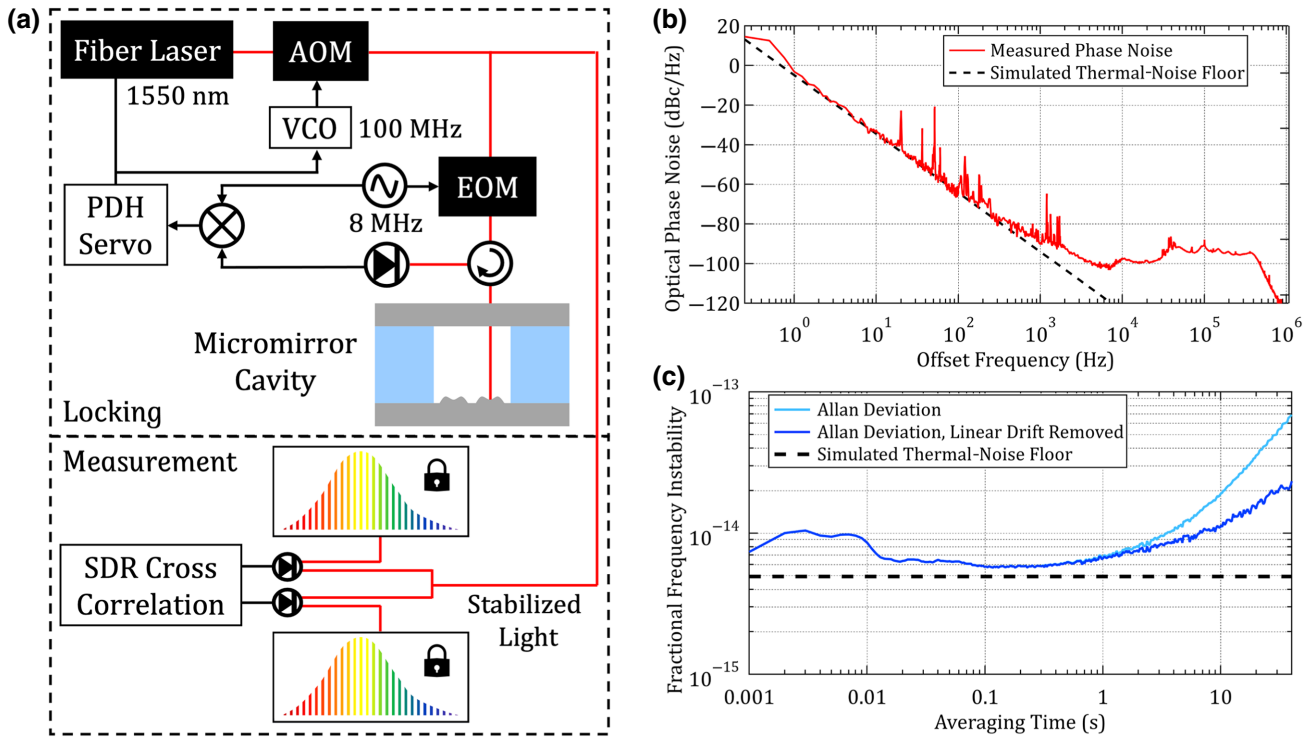
FIG. 4. (a) Experimental setup for PDH locking and phase-noise measurement. PDH, Pound-Drever-Hall; VCO, voltage-controlled oscillator; AOM, acousto-optic modulator; EOM, electro-optic modulator; SDR, software-defined radio. (b) Phase noise measurement of the stabilized light. Rolloff above 400 kHz is a measurement artifact. (c) Fractional frequency instability with and without removal of 1.3 Hz/s linear drift. The effective bandwidth of this measurement is 2 kHz.

offset, confirming that the micromirror fabrication process does not substantially alter the high mechanical Q_M of the fused silica substrate and demonstrating the utility of these micromirrors for low-noise laser stabilization. The noise at higher offset frequencies is dominated by unsuppressed noise of the fiber laser, limited by the finite gain bandwidth of the feedback control loop. Finally, to document the longer-term stability of the cavity, the Allan deviation is extracted from the phase record of one of the two heterodyne beat notes sampled with SDR [Fig. 4(c)]. At 1 s, the Allan deviation is 7×10^{-15}. Following removal of a 1.3 Hz/s linear drift, the fractional frequency instability is shown to be 10^{-14} or better out to 7 s of averaging, after which nonlinear drift dominates. In future cavities, this drift could be reduced by operating at a zero-crossing temperature of the effective cavity CTE.

IV. CONCLUSION

These results demonstrate ultrastable laser performance from a cm-scale compact cavity using lithographically fabricated mirrors. Finite-element noise modeling indicates that the volume can be reduced from the 8-ml volume used here to 2 ml without sacrificing the noise performance by simply reducing the cavity's cross-section diameter. With consistently high finesse across all three micromirrors, we

show that this scalable microfabrication technique maintains very high surface quality, with minimal excess losses due to absorption, scattering, or clipping from poor alignment tolerances or micromirror shape. The finesse values obtained for all three micromirrors are consistent with total excess loss of less than 2 ppm per mirror. Similarly high finesse and low loss (1–2 ppm) are also measured on two other 10-mm-long bonded micromirror cavities, which will be described in future publications. Furthermore, the thermal-noise-limited performance out to approximately 1-kHz offset confirms that the mirror fabrication technique does not significantly degrade the fused silica substrate's naturally high mechanical Q_M. Finally, the fractional frequency instability reaches 6×10^{-15} between 0.1 and 1 s, and remains below 10^{-14} out to several seconds of averaging, making this cavity useful for portable optical clock applications.

In order for a new generation of stable, portable frequency references to proliferate to the wide range of field applications that have long been dominated by quartz-based oscillators, a path towards scalable manufacturing is required. We envision fabricating many micromirror-based Fabry-Perot cavities in parallel: by patterning a grid of micromirrors onto a single substrate, bonding this with a spacer possessing a matching grid of bore holes, and capping the other end with a flat mirror substrate, we

could simultaneously assemble a large number of reference cavities in a single bonded assembly. Along with the demonstrated angstrom-level roughness of the mirror substrates, recent work [52] suggests that bond strength can be sufficient to then dice up the grid of reference cavities into individual units. As with all ultrastable laser systems, a small overall system size (including vacuum and temperature stabilization) is essential for implementation in portable applications. In future work, we aim to integrate these compact reference cavities into fully engineered compact housings to facilitate operation outside of laboratory environments. Here, we take a step towards the mass manufacture of portable, ultrastable Fabry-Perot reference cavities by demonstrating better than 10^{-14} instability and thermally limited performance over several decades using micromirrors fabricated in a highly repeatable lithographic process.

The data that support the findings of this study are available from the corresponding author upon reasonable request.

[1] A. D. Ludlow, M. M. Boyd, J. Ye, E. Peik, and P. O. Schmidt, Optical atomic clocks, Rev. Mod. Phys. **87**, 637 (2015).

[2] E. Oelker, R. Hutson, C. Kennedy, L. Sonderhouse, T. Bothwell, A. Goban, D. Kedar, C. Sanner, J. Robinson, G. Marti, *et al.*, Demonstration of 4.8×10^{-17} stability at 1 s for two independent optical clocks, Nat. Photonics **13**, 714 (2019).

[3] W. McGrew, X. Zhang, R. Fasano, S. Schäffer, K. Beloy, D. Nicolodi, R. Brown, N. Hinkley, G. Milani, M. Schioppo, *et al.*, Atomic clock performance enabling geodesy below the centimetre level, Nature **564**, 87 (2018).

[4] T. Takano, M. Takamoto, I. Ushijima, N. Ohmae, T. Akatsuka, A. Yamaguchi, Y. Kuroishi, H. Munekane, B. Miyahara, and H. Katori, Geopotential measurements with synchronously linked optical lattice clocks, Nat. Photonics **10**, 662 (2016).

[5] B. Willke, K. Danzmann, M. Frede, P. King, D. Kracht, P. Kwee, O. Puncken, R. Savage, B. Schulz, F. Seifert, *et al.*, Stabilized lasers for advanced gravitational wave detectors, Classical Quantum Gravity **25**, 114040 (2008).

[6] T. M. Fortier, M. S. Kirchner, F. Quinlan, J. Taylor, J. Bergquist, T. Rosenband, N. Lemke, A. Ludlow, Y. Jiang, C. Oates, *et al.*, Generation of ultrastable microwaves via optical frequency division, Nat. Photonics **5**, 425 (2011).

[7] X. Xie, R. Bouchand, D. Nicolodi, M. Giunta, W. Hänsel, M. Lezius, A. Joshi, S. Datta, C. Alexandre, M. Lours, *et al.*, Photonic microwave signals with zeptosecond-level absolute timing noise, Nat. Photonics **11**, 44 (2017).

[8] P. Lu, N. Lalam, M. Badar, B. Liu, B. T. Chorpening, M. P. Buric, and P. R. Ohodnicki, Distributed optical fiber sensing: Review and perspective, Appl. Phys. Rev. **6**, 041302 (2019).

[9] L. Shi, T. Zhu, Q. He, and S. Huang, in *23rd International Conference on Optical Fibre Sensors*, Vol. 9157 (Proc. SPIE, Santander, Spain, 2014), p. 91576H.

[10] N. Huntemann, B. Lipphardt, C. Tamm, V. Gerginov, S. Weyers, and E. Peik, Improved Limit on a Temporal Variation of m_p/m_e from Comparisons of Yb^+ and Cs Atomic Clocks, Phys. Rev. Lett. **113**, 210802 (2014).

[11] P. Delva, J. Lodewyck, S. Bilicki, E. Bookjans, G. Vallet, R. Le Targat, P.-E. Pottie, C. Guerlin, F. Meynadier, C. Le Poncin-Lafitte, *et al.*, Test of Special Relativity using a Fiber Network of Optical Clocks, Phys. Rev. Lett. **118**, 221102 (2017).

[12] A. Derevianko and M. Pospelov, Hunting for topological dark matter with atomic clocks, Nat. Phys. **10**, 933 (2014).

[13] Y. Stadnik and V. Flambaum, Searching for Dark Matter and Variation of Fundamental Constants with Laser and Maser Interferometry, Phys. Rev. Lett. **114**, 161301 (2015).

[14] P. Ghelfi, F. Laghezza, F. Scotti, G. Serafino, A. Capria, S. Pinna, D. Onori, C. Porzi, M. Scaffardi, A. Malacarne, *et al.*, A fully photonics-based coherent radar system, Nature **507**, 341 (2014).

[15] J. A. Scheer and J. L. Kurtz, *Coherent Radar Performance Estimation* (Artech House, Boston, 1993).

[16] F. Riehle, Towards a redefinition of the second based on optical atomic clocks, C. R. Phys. **16**, 506 (2015).

[17] J. Grotti, S. Koller, S. Vogt, S. Häfner, U. Sterr, C. Lisdat, H. Denker, C. Voigt, L. Timmen, A. Rolland, *et al.*, Geodesy and metrology with a transportable optical clock, Nat. Phys. **14**, 437 (2018).

[18] M. Takamoto, I. Ushijima, N. Ohmae, T. Yahagi, K. Kokado, H. Shinkai, and H. Katori, Test of general relativity by a pair of transportable optical lattice clocks, Nat. Photonics **14**, 411 (2020).

[19] G. Marra, C. Clivati, R. Luckett, A. Tampellini, J. Kronjäger, L. Wright, A. Mura, F. Levi, S. Robinson, A. Xuereb, *et al.*, Ultrastable laser interferometry for earthquake detection with terrestrial and submarine cables, Science **361**, 486 (2018).

[20] J. Sanjuan, K. Abich, M. Gohlke, A. Resch, T. Schuldt, T. Wegehaupt, G. P. Barwood, P. Gill, and C. Braxmaier, Long-term stable optical cavity for special relativity tests in space, Opt. Express **27**, 36206 (2019).

[21] D. Matei, T. Legero, S. Häfner, C. Grebing, R. Weyrich, W. Zhang, L. Sonderhouse, J. Robinson, J. Ye, F. Riehle, *et al.*, 1.5 μm Lasers with Sub-10 mHz Linewidth, Phys. Rev. Lett. **118**, 263202 (2017).

[22] J. G. Hartnett, N. R. Nand, and C. Lu, Ultra-low-phase-noise cryocooled microwave dielectric-sapphire-resonator oscillators, Appl. Phys. Lett. **100**, 183501 (2012).

[23] J. Chauvin, P. Weber, J.-P. Aubry, F. Lefebvre, F. Sthal, S. Galliou, E. Rubiola, and X. Vacheret, in *2007 IEEE International Frequency Control Symposium Joint with the 21st European Frequency and Time Forum* (IEEE, Geneva, Switzerland, 2007), p. 1261.

[24] D. T. Spencer, *et al.*, An optical-frequency synthesizer using integrated photonics, Nature **557**, 81 (2018).

[25] H. Lee, M.-G. Suh, T. Chen, J. Li, S. A. Diddams, and K. J. Vahala, Spiral resonators for on-chip laser frequency stabilization, Nat. Commun. **4**, 1 (2013).

[26] W. Zhang, F. Baynes, S. A. Diddams, and S. B. Papp, Microrod Optical Frequency Reference in the Ambient Environment, Phys. Rev. Appl. **12**, 024010 (2019).

[27] L. Stern, W. Zhang, L. Chang, J. Guo, C. Xiang, M. A. Tran, D. Huang, J. D. Peters, D. Kinghorn, J. E. Bowers, *et al.*, Ultra-precise optical-frequency stabilization with heterogeneous III–V/Si lasers, Opt. Lett. **45**, 5275 (2020).

[28] W. Loh, J. Stuart, D. Reens, C. D. Bruzewicz, D. Braje, J. Chiaverini, P. W. Juodawlkis, J. M. Sage, and R. McConnell, Operation of an optical atomic clock with a Brillouin laser subsystem, Nature **588**, 244 (2020).

[29] J. Alnis, A. Schliesser, C. Y. Wang, J. Hofer, T. J. Kippenberg, and T. Hänsch, Thermal-noise-limited crystalline whispering-gallery-mode resonator for laser stabilization, Phys. Rev. A **84**, 011804 (2011).

[30] J. Lim, A. A. Savchenkov, E. Dale, W. Liang, D. Eliyahu, V. Ilchenko, A. B. Matsko, L. Maleki, and C. W. Wong, Chasing the thermodynamical noise limit in whispering-gallery-mode resonators for ultrastable laser frequency stabilization, Nat. Commun. **8**, 1 (2017).

[31] J. Davila-Rodriguez, F. N. Baynes, A. D. Ludlow, T. M. Fortier, H. Leopardi, S. A. Diddams, and F. Quinlan, Compact, thermal-noise-limited reference cavity for ultra-low-noise microwave generation, Opt. Lett. **42**, 1277 (2017).

[32] D. R. Leibrandt, J. C. Bergquist, and T. Rosenband, Cavity-stabilized laser with acceleration sensitivity below 10^{-12} g^{-1}, Phys. Rev. A **87**, 023829 (2013).

[33] A. Didier, J. Millo, B. Marechal, C. Rocher, E. Rubiola, R. Lecomte, M. Ouisse, J. Delporte, C. Lacroûte, and Y. Kersalé, Ultracompact reference ultralow expansion glass cavity, Appl. Opt. **57**, 6470 (2018).

[34] S. Webster and P. Gill, Force-insensitive optical cavity, Opt. Lett. **36**, 3572 (2011).

[35] P. Kharel, Y. Chu, M. Power, W. H. Renninger, R. J. Schoelkopf, and P. T. Rakich, Ultra-high-Q phononic resonators on-chip at cryogenic temperatures, APL Photonics **3**, 066101 (2018).

[36] N. Jin, C. A. McLemore, D. Mason, J. P. Hendrie, Y. Luo, M. L. Kelleher, P. Kharel, F. Quinlan, S. A. Diddams,

and P. T. Rakich, Micro-fabricated mirrors with finesse exceeding one million, Optica **9**, 965 (2022).

[37] Y. Levin, Internal thermal noise in the LIGO test masses: A direct approach, Phys. Rev. D **57**, 659 (1998).

[38] T. Kessler, T. Legero, and U. Sterr, Thermal noise in optical cavities revisited, JOSA B **29**, 178 (2012).

[39] Y. T. Liu and K. S. Thorne, Thermoelastic noise and homogeneous thermal noise in finite sized gravitational-wave test masses, Phys. Rev. D **62**, 122002 (2000).

[40] M. Cerdonio, L. Conti, A. Heidmann, and M. Pinard, Thermoelastic effects at low temperatures and quantum limits in displacement measurements, Phys. Rev. D **63**, 082003 (2001).

[41] M. Evans, S. Ballmer, M. Fejer, P. Fritschel, G. Harry, and G. Ogin, Thermo-optic noise in coated mirrors for high-precision optical measurements, Phys. Rev. D **78**, 102003 (2008).

[42] H. B. Callen and T. A. Welton, Irreversibility and generalized noise, Phys. Rev. **83**, 34 (1951).

[43] T. Legero, T. Kessler, and U. Sterr, Tuning the thermal expansion properties of optical reference cavities with fused silica mirrors, JOSA B **27**, 914 (2010).

[44] E. D. Black, An introduction to Pound–Drever–Hall laser frequency stabilization, Am. J. Phys. **69**, 79 (2001).

[45] W. Zhang, M. Martin, C. Benko, J. Hall, J. Ye, C. Hagemann, T. Legero, U. Sterr, F. Riehle, G. Cole, *et al.*, Reduction of residual amplitude modulation to 1×10^{-6} for frequency modulation and laser stabilization, Opt. Lett. **39**, 1980 (2014).

[46] C. J. Hood, H. Kimble, and J. Ye, Characterization of high-finesse mirrors: Loss, phase shifts, and mode structure in an optical cavity, Phys. Rev. A **64**, 033804 (2001).

[47] D. Z. Anderson, J. C. Frisch, and C. S. Masser, Mirror reflectometer based on optical cavity decay time, Appl. Opt. **23**, 1238 (1984).

[48] G. D. Cole, W. Zhang, M. J. Martin, J. Ye, and M. Aspelmeyer, Tenfold reduction of Brownian noise in high-reflectivity optical coatings, Nat. Photonics **7**, 644 (2013).

[49] R. Drever, J. L. Hall, F. Kowalski, J. Hough, G. Ford, A. Munley, and H. Ward, Laser phase and frequency stabilization using an optical resonator, Appl. Phys. B **31**, 97 (1983).

[50] T. Nakamura, J. Davila-Rodriguez, H. Leopardi, J. A. Sherman, T. M. Fortier, X. Xie, J. C. Campbell, W. F. McGrew, X. Zhang, Y. S. Hassan, *et al.*, Coherent optical clock down-conversion for microwave frequencies with 10^{-18} instability, Science **368**, 889 (2020).

[51] J. A. Sherman and R. Jördens, Oscillator metrology with software defined radio, Rev. Sci. Instrum. **87**, 054711 (2016).

[52] P. Birckigt, K. Grabowski, G. Leibeling, T. Flügel-Paul, M. Heusinger, H. Ouslimani, and S. Risse, Effects of static load and residual stress on fused silica direct bonding interface properties, Appl. Phys. A **127**, 1 (2021).